

Connection between orbital modulation of $H\alpha$ and gamma-rays in the Be/X-ray binary LS I+61°303

R. Zamanov¹, J. Martí², K. Stoyanov¹, A. Borissova¹, and N. A. Tomov¹

¹ Institute of Astronomy and National Astronomical Observatory, Bulgarian Academy of Sciences, 72 Tsarigradsko Shose Blvd., 1784 Sofia, Bulgaria

e-mail: rkz@astro.bas.bg, jmarti@ujaen.es, kstoyanov@astro.bas.bg, tomov@astro.bas.bg

² Departamento de Física (EPSJ), Universidad de Jaén, Campus Las Lagunillas, A3-420, 23071, Jaén, Spain

Received November 1, 2013; accepted, 2014

ABSTRACT

We studied the average orbital modulation of various parameters (γ -ray flux, $H\alpha$ emission line, optical V band brightness) of the radio- and γ -ray emitting Be/X-ray binary LS I+61°303. Using the Spearman rank correlation test, we found highly significant correlations between the orbital variability of the equivalent width of the blue hump of the $H\alpha$ and *Fermi*-LAT flux with a Spearman p-value $\sim 2 \times 10^{-5}$, and the equivalent widths ratio EW_B/EW_R and *Fermi*-LAT flux with p-value $\sim 9 \times 10^{-5}$. We also found a significant anti-correlation between *Fermi*-LAT flux and V band magnitude with p-value $\sim 7 \times 10^{-4}$.

All these correlations refer to the average orbital variability, and we conclude that the $H\alpha$ and γ -ray emission processes in LS I+61°303 are connected. The possible physical scenario is briefly discussed.

Key words. Stars: individual: LS I+61°303 – Gamma rays: stars – X-rays: binaries – Stars: winds, outflows

1. Introduction

LS I+61°303 (V615 Cas) is a high-mass X-ray binary whose remarkable nature was illustrated following the discovery of its strong, non-thermal, and periodic radio outbursts (Gregory & Taylor 1978). It was first detected as a strong γ -ray source by the *COS B* satellite (Hermsen et al. 1977). More recently, it has also been reported as a source of high-energy (HE) and very high-energy (VHE) γ -rays by the *Fermi* Large Area Telescope (LAT, Abdo et al. 2009), the MAGIC Cherenkov telescope (Albert et al. 2006), and by the VERITAS collaboration (Maier et al. 2012). Indeed, it is currently considered one of the few confirmed representatives of the selected class of γ -ray binaries since the system's luminosity in this energy range dominates the whole spectral energy distribution.

LS I+61°303 consists of a massive B0Ve star and a compact object orbiting the primary every 26.5 d. According to the most recent radial velocity measurements of the absorption lines of the primary (Casares et al. 2005, Aragona et al. 2009), the orbit is elliptical ($e = 0.537 \pm 0.034$), with periastron passage determined to occur around phase $\phi = 0.275$. The compact object interacts with the Be circumstellar disk thereby sampling a wide range of physical parameters and producing remarkable, periodic flaring events each orbital cycle. Such a strong orbital modulation in the LS I+61°303 emission is observed across the whole electromagnetic spectrum, especially in the radio (Taylor et al. 1992), optical (Mendelson & Mazeh 1994), X-ray (Paredes et al. 1997, Leahy 2001), HE (Abdo et al. 2009), and VHE γ -ray (Albert et al. 2009) domains. In the optical, the orbital period signature is evident not only in visible broad band photometry, but also in the spectral properties of the $H\alpha$ emission line (Zamanov et al. 1999; Grundstrom et al. 2007). The scenario of compact companion interaction with the Be disk is currently favored by

Very Long Baseline Interferometry (VLBI) images that show a cometary structure on milli-arcsecond angular scales that rotates with the orbital period (Dhawan et al. 2006).

In addition to the orbital periodicity, another clock is operating in the system. A periodic modulation of about 4.4 yr in the phase and amplitude of the radio outbursts was first reported by Paredes (1987) and Gregory et al. (1989). This super-orbital modulation has also been detected in $H\alpha$ (Zamanov et al. 1999), X-rays (Li et al. 2012), and γ -rays (Ackermann et al. 2013). It could be due to precession of the Be disk (Lipunov & Nazin 1994), a beat frequency between the orbital and precessional rates (Massi & Jaron 2013), or quasi-cyclical variability of the equatorial outflow of the Be star.

Previous multiwavelength observations have revealed interesting correlations between the X-ray and VHE gamma-ray flares (Albert et al. 2008, Anderhub et al. 2009). This suggests that the same relativistic electrons that radiate inverse Compton VHE photons also produce synchrotron X-ray emission. In this Letter, we further explore the multiwavelength behavior of LS I+61°303 in different spectral domains and search for correlations among them that could help to better characterize the physical mechanism behind the system's orbital flaring episodes. In particular, we focus our attention on the two LS I+61°303 extensive observational monitorings that are currently available, namely in γ -rays and in $H\alpha$ high-resolution spectroscopy. Other observational databases in the radio and optical domains are also included in our study.

2. Observations

To create the folded light curve of LS I+61°303, we used the following data:

For **HE γ -rays**, the *Fermi* team monitors flux values for a number of bright sources and transient sources that cross their monitoring flux threshold. Here we downloaded the *Fermi* LAT daily-averaged flux values for LS I+61°303 in the energy range from 0.1 to 300 GeV. At the time of writing, this data set covered the time interval from JD 2454688.5 (2008 August) to JD 2456358.5 (2013 March).

Johnson V band magnitudes were taken from Lipunova (1988), Paredes et al. (1994), Zaitseva & Borisov (2003). Among the photometry available in the literature, we used only those observations that are reduced to Johnson's system. We also calculated average orbital variability using the unfiltered optical magnitudes (149 measurements) from the Northern Sky Variability Survey (Woźniak et al. 2004). These unfiltered magnitudes are not plotted here, but they do confirm the detected V band variability.

H α spectroscopic data were taken from Paredes et al. (1994), Steele et al. (1996), Liu & Yan (2005), Grundstrom et al. (2007), McSwain et al. (2010), and Zamanov et al. (1999, 2013). Among the various parameters of the H α emission line we used here are the total equivalent width of the H α emission line, hereafter *EW*, the equivalent width of the blue hump *EW(B)*, the equivalent width of the red hump *EW(R)*, the ratio between the equivalent widths of the blue and red humps *EW_B/EW_R*, and the distance between the peaks, ΔV_p .

In **radio photometry**, flux densities were retrieved from the old Green Bank Interferometer (GBI), which is a facility of the USA National Science Foundation operated by NRAO in support of the NASA High Energy Astrophysics program. A total of 7234 observations of the flux density at 2.25 GHz and 8.3 GHz obtained from JD2450410 (November 1996) until 2451664 (April 2000) are available for study.

3. Orbital variability of different parameters

The orbital phase is calculated using $P_{orb} = 26.4960 \pm 0.0028$ days, a value derived from Bayesian analysis of the radio observations (Gregory 2002). The zero of phase is by convention $JD_0 = 2,443,366.775$, the date of the first radio detection of the star (Gregory & Taylor 1978).

To calculate the average orbital variability, we separated the data in 20 non-overlapping bins. The bins are all of the same size – 0.05 in phase each. In each phase bin we calculated the average value, median value, and standard deviation of the mean. The values were calculated separately for every data type. In this way we obtained 20 points per orbital period and plotted them in Fig. 1. The data are repeated over two cycles for clarity. In Fig. 1 from top to bottom we plot

- a-** radio flux density at 2.25 GHz (in Jy),
- b-** radio flux density at 8.3 GHz (in Jy),
- c-** the distance between the peaks of the H α emission line, ΔV_p , in km s^{-1} ,
- d-** equivalent width of the blue hump of H α , *EW(B)*, in \AA ,
- e-** equivalent width of the red hump of H α , *EW(R)*, in \AA ,
- f-** the dimensionless ratio between equivalent widths of the blue and red humps of H α *EW_B/EW_R*,
- g-** the total equivalent width of H α emission line, *EW(H α)*, in \AA ,
- h-** the optical (Johnson) V band magnitude,
- k-** the *Fermi*-LAT photon flux in the 0.1-300 GeV energy range (in units 10^{-7} photons $\text{cm}^{-2} \text{s}^{-1}$).

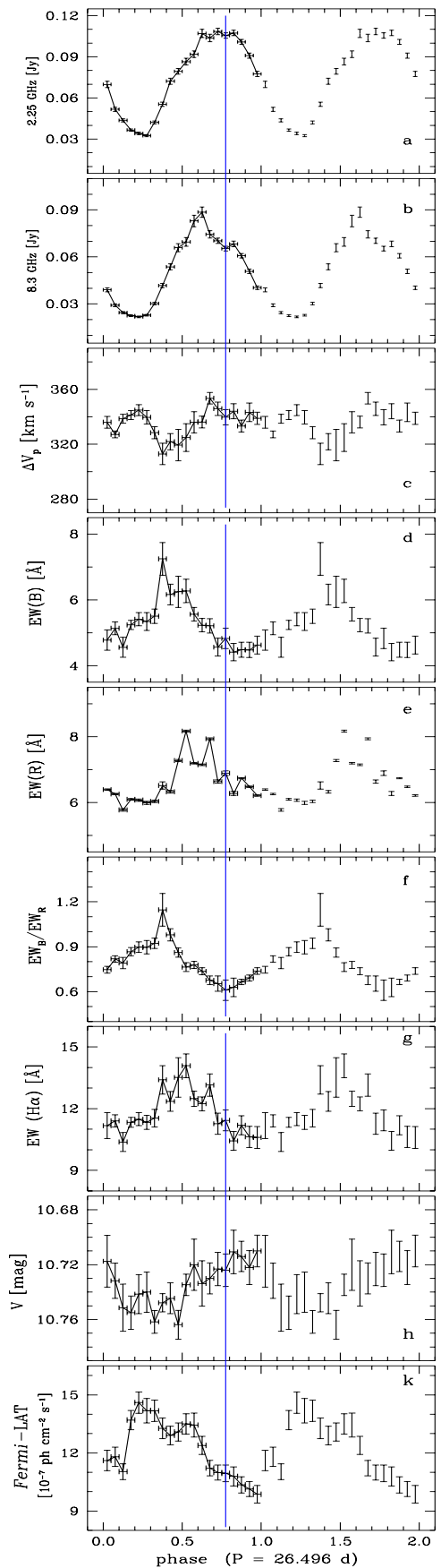


Fig. 1. The averaged orbital variability of LS I+61°303. Plotted from up to down: the radio fluxes at 2.25 and 8.3 GHz, ΔV_p , *EW(B)*, *EW(R)*, *EW_B/EW_R*, *EW(H α)*, the optical V, and the *Fermi*-LAT flux. The vertical (blue) line indicates the apastron passage. The data are averaged in 20 bins that are 0.05 each.

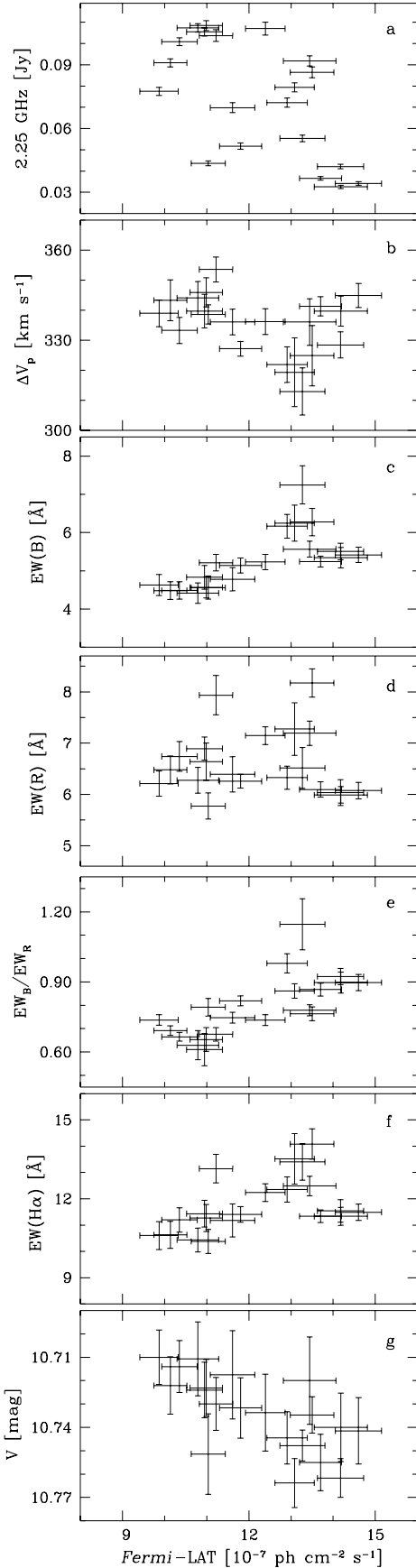


Fig. 2. Various parameters plotted versus *Fermi*-LAT flux. Plotted from up to down: 2.25 GHz, ΔV_p , EW(B), EW(R), the ratio EW_B/EW_R , EW(H α), and V magnitude. Each point represents 1 bin with size 0.05 (see also Fig.1 and Table 1).

Table 1. Spearman’s (rho) correlation test results.

Parameters	Spearman test coeff.	p-value	Result	Fig.
γ - radio	0.12	$6.3 \cdot 10^{-1}$		2a
γ - ΔV_p	-0.32	$1.6 \cdot 10^{-1}$		2b
γ - EW(B)	0.80	$2.1 \cdot 10^{-5}$	highly sign.	2c
γ - EW(R)	-0.16	$4.7 \cdot 10^{-1}$		2d
γ - EW_B/EW_R	0.76	$8.8 \cdot 10^{-5}$	highly sign.	2e
γ - EW(H α)	0.58	$6.7 \cdot 10^{-3}$	significant	2f
γ - V	0.69	$7.0 \cdot 10^{-4}$	highly sign.	2g
EW(B) - V	0.65	$2.1 \cdot 10^{-3}$	significant	
EW(R) - V	-0.23	$3.2 \cdot 10^{-1}$		
EW(H α) - V	0.45	$4.6 \cdot 10^{-2}$		

γ = *Fermi*-LAT flux.

In this figure, it can be seen that the minimum of the γ -ray production is around the time of the apastron and after it. This corresponds to the maximum of the optical V brightness. At the same orbital phases a very pronounced minimum is visible in EW(H α), EW(B), and EW_B/EW_R .

3.1. Phase lags

In Fig. 1 it is visible that the averaged radio fluxes peak at phase ~ 0.7 , while V magnitude peaks at phase ~ 0.9 , EW(H α) at phase ~ 0.5 , EW(B) at phase ~ 0.4 , *Fermi*-LAT flux at phase ~ 0.3 .

To estimate the phase shift between the different bands, we used a cross correlation function (CCF) with the *Fermi*-LAT flux as a reference. The delay of the other parameters is as follows: radio flux at 2.25 GHz is delayed by 0.36, radio flux at 8.3 GHz is delayed by 0.30, V band brightness is delayed by 0.47, EW(H α) is delayed by 0.14, EW(B) is delayed by 0.06, and EW(R) is delayed by 0.28. The typical error of these shifts is ± 0.03 .

3.2. Correlations: H α , V magnitude, and radio versus γ -rays

The various optical and radio parameters are plotted versus *Fermi*-LAT flux in Fig. 2. In each panel there are 20 data points, plotted with their errors. For each panel of this figure we performed Spearman’s (rho) rank correlation test. The results of the test (correlation coefficient and p-value) are summarized in Table 1, where the first column lists the correlated parameters, and the second the correlation coefficient and its significance (p-value). The third column notes our result, and if no correlation is detected it is empty. The fourth column refers to the figure where the data are plotted.

The highest correlations are between *Fermi*-LAT and EW(B), as well as *Fermi*-LAT and EW_B/EW_R . It is worth noting that EW_B/EW_R is one of the H α emission parameters where the orbital period is most visible (Zamanov et al. 2013). The correlation is also highly significant ($p < 0.001$) for γ -rays and EW(B) and for γ -rays and the optical V band magnitude. Between γ -rays and the optical V band, there is an anti-correlation, and the optical brightness decreases when the γ flux increases. There is also a correlation between *Fermi*-LAT flux and total EW(H α), which seems to be significant ($p \leq 0.01$). The sta-

tistical significance of the correlations, with chance probability values $p \approx 10^{-4}$, indicates a relationship between the $H\alpha$ and γ -ray emission processes.

It is worth noting that (i) there is no correlation between the $EW(H\alpha)$ and V . However, a correlation does exist between $EW(B)$ and V brightness. (ii) If we use the phase lags to match up the orbital modulation, the Spearman test gives a worse result for $\gamma - EW(B)$ (0.76 , $p = 1.0 \cdot 10^{-4}$), better result for $\gamma - EW_B/EW_R$ (0.78 , $p = 4.1 \cdot 10^{-5}$), considerably better result for $\gamma - EW(H\alpha)$ (0.80 , $p = 2.2 \cdot 10^{-5}$), and an even better result for $\gamma - V$ (0.75 , $p = 1.5 \cdot 10^{-4}$), in comparison with the values in Table 1.

4. Discussion and conclusions

The type of the secondary in LS I+61°303 is still unknown. Several models have been proposed for the nature of the compact object in LS I+61°303 several models have been proposed: an accreting black hole launching relativistic jets (microquasar, e.g., Massi et al. 2012), rotation-powered pulsar (Dubus 2013), ejector-propeller (Zamanov et al. 2001), and accretor-ejector model (Maraschi & Treves 1981). The properties of the short bursts recently observed are typical of those shown by high magnetic field neutron stars (magnetars), so they provide one more indication of neutron star (Papitto, Torres & Rea 2012). During the ejector stage (pulsar) the gamma ray emission is thought to originate in the shock front at the boundary of the pulsar and stellar winds and/or inverse Compton process. Electrons and hadrons can also be accelerated to relativistic energies by a propeller-acting neutron star (accretion onto the magnetosphere of magnetar). These relativistic particles will produce γ -ray and neutrino emission (see Bednarek 2011, and references therein).

The $H\alpha$ emission in Be stars and Be/X-ray binaries is coming from a Keplerian disk around the Be star (e.g., Hanuschik et al. 1988). This circumstellar disk also supplies the material that feeds the accretion onto the X-ray pulsars in the Be/X-ray binaries.

Phase lags: We detected and calculated the phase lags between γ -rays from one side and optical, $H\alpha$, and radio parameters from the other side (see Sect.3.1 and Fig.1). Chernyakova et al. (2012) used simultaneous X-ray and radio observations to show that periodic radio flares always lag behind the X-ray flare by $\Delta\phi \approx 0.2$, a behavior predicted by the ejector - propeller model. The radio outbursts are probably due to an expansion of a synchrotron emitting source (plasmon), with a prolonged injection of energetic particles (Paredes et al. 1991). In this model the phase shifts between the high-energy emission and other bands are probably connected with the ejection of relativistic wind (or jets) from the compact object, the appearance, and the expansion of the plasmon, which achieves the maximum of the radio flux a few (2 - 8) days after its appearance.

Correlations: We detected a highly significant anti-correlation between *Fermi*-LAT flux and optical V brightness. This could be due to changes in the ionization in the Be circumstellar disk in response to the high-energy emission, which changes the opacity and the emission. The gamma-ray bright blazars in the sample of Bonning et al. (2012) have optical emission correlated with gamma-rays. Bonning et al. (2012) suggest that this strongly supports leptonic models for the gamma-ray production. We have the opposite situation, which is hard to reconcile with leptonic models based on the inverse Compton origin of the *Fermi*-LAT photons from LS I+61°303.

The *Fermi*-LAT flux achieves the maximum at about the time of the periastron passage. The highest values of the $EW(B)$ are reached in the phase interval 0.3 - 0.6. The highest values

of EW_B/EW_R are about the orbital phase 0.40. The highest values of the total $EW(H\alpha)$ are also reached in the phase interval 0.3 - 0.6. That the *Fermi*-LAT flux correlates with $EW(B)$ and EW_B/EW_R , and not with $EW(R)$ indicates that the high-energy emission does not influence all the Be disk but only the vicinity around the compact object.

For rotationally dominated profiles the peak separation can be regarded as a measure of the outer radius (e.g., Hanuschik et al. 1988). Because there is no correlation of *Fermi*/LAT flux and ΔV_p , it means that the size of the $H\alpha$ emitting disk does not respond to the changes of the γ -ray flux. This agrees with the above that only the surroundings of the compact object star are involved.

Conclusions: We detected highly significant correlations (chance probability value $\approx 10^{-4}$) between the orbital modulation of the blue hump of $H\alpha$ emission line and *Fermi*-LAT flux and between the ratio EW_B/EW_R and *Fermi*-LAT flux, as well as an anti-correlation between V band brightness and *Fermi*-LAT flux. This implies a direct link between the $H\alpha$ and γ -ray emission processes.

Acknowledgements. We are very grateful to the referee, E. Grundstrom, for valuable comments. This work was partially supported the OP "HRD", ESF, and Bulgarian Ministry of Education and Science (BG051PO001-3.3.06-0047). JM acknowledges support by grant AYA2010-21782-C03-03 from the Spanish Government, and Consejería de Economía, Innovación y Ciencia of Junta de Andalucía as research group FQM-322, as well as FEDER funds.

References

- Abdo, A. A., Ackermann, M., Ajello, M., et al. 2009, *ApJ*, 701, L123
 Ackermann, M., Ajello, M., Ballet, J., et al. 2013, *ApJ*, 773, L35
 Albert, J., Aliu, E., Anderhub, H., et al. 2006, *Science*, 312, 1771
 Albert, J., Aliu, E., Anderhub, H., et al. 2008, *ApJ*, 684, 1351
 Albert, J., Aliu, E., Anderhub, H., et al. 2009, *ApJ*, 693, 303
 Anderhub, H., Antonelli, L. A., Antoranz, P., et al. 2009, *ApJ*, 706, 27
 Aragona, C., McSwain, M. V., Grundstrom, E. D., et al. 2009, *ApJ*, 698, 514
 Bednarek, W. 2011, *IAU Symposium*, 275, 305
 Bonning, E., Urry, C. M., Bailyn, C., et al. 2012, *ApJ*, 756, 13
 Casares, J., Ribas, I., Paredes, J. M., Martí, J., & Allende Prieto, C. 2005, *MNRAS*, 360, 1105
 Chernyakova, M., Neronov, A., Molokov, S., et al. 2012, *ApJ*, 747, L29
 Dubus, G. 2013, *A&A Rev.*, 21, 64
 Dhawan, V., Mioduszewski, A., & Rupen, M. 2006, in *Proc. VI Microquasar Workshop: Microquasars and Beyond*, ed. T. Belloni (Trieste: PoS), 52
 Gregory, P. C., & Taylor, A. R. 1978, *Nature*, 272, 704
 Gregory, P. C. 2002, *ApJ*, 575, 427
 Gregory, P. C., Xu, H.-J., Backhouse, C. J., & Reid, A. 1989, *ApJ*, 339, 1054
 Grundstrom, E. D., Caballero-Nieves, S. M., Gies, D. R., et al. 2007, *ApJ*, 656, 437
 Hanuschik, R. W., Kozok, J. R., & Kaiser, D. 1988, *A&A*, 189, 147
 Hermesen, W., Swannenburg, B. N., Bignami, G. F., et al. 1977, *Nature*, 269, 494
 Leahy, D. A. 2001, *A&A*, 380, 516
 Li, J., Torres, D. F., Zhang, S., et al. 2012, *ApJ*, 744, L13
 Lipunov, V. M., & Nazin, S. N. 1994, *A&A*, 289, 822
 Lipunova, N. A. 1988, *Soviet Ast.*, 32, 52
 Liu, Q. Z., & Yan, J. Z. 2005, *New A*, 11, 130
 Maier, G., & VERITAS Collaboration 2012, *American Institute of Physics Conference Series*, 1505, 362
 Maraschi, L., & Treves, A. 1981, *MNRAS*, 194, 1P
 Massi, M., Ros, E., & Zimmermann, L. 2012, *A&A*, 540, A142
 Massi, M., & Jaron, F. 2013, *A&A*, 554, A105
 McSwain, M. V., Grundstrom, E. D., Gies, D. R., & Ray, P. S. 2010, *ApJ*, 724, 379
 Papitto, A., Torres, D. F., & Rea, N. 2012, *ApJ*, 756, 188
 Paredes, J. M., 1987, PhD thesis, University of Barcelona
 Paredes, J. M., Martí, J., Estalella, R., & Sarrate, J. 1991, *A&A*, 248, 124
 Paredes, J. M., Martí, J., Peracaula, M., & Ribo, M. 1997, *A&A*, 320, L25
 Paredes, J. M., Marziani, P., Martí, J., et al. 1994, *A&A*, 288, 519
 Romero, G. E., Okazaki, A. T., Orellana, M., & Owocki, S. P. 2007, *A&A*, 474, 15
 Steele, I. A., Coe, M. J., Fabregat, J., et al. 1996, *A&AS*, 120, 213
 Taylor, A. R., Kenny, H. T., Spencer, R. E., & Tzioumis, A. 1992, *ApJ*, 395, 268
 Torres, D. F., Zhang, S., Li, J., et al. 2010, *ApJ*, 719, L104
 Woźniak, P. R., Vestrand, W. T., Akerlof, C. W., et al. 2004, *AJ*, 127, 2436
 Wynn, G. A., King, A. R., & Horne, K. 1997, *MNRAS*, 286, 436
 Zaitseva, G. V., & Borisov, G. V. 2003, *Astronomy Letters*, 29, 188
 Zamanov, R. K., Martí, J., Paredes, J. M., et al. 1999, *A&A*, 351, 543
 Zamanov, R., Martí, J., & Marziani, P. 2001, *The Second National Conference on Astrophysics of Compact Objects*, 50 (astro-ph/0110114)
 Zamanov, R., Stoyanov, K., Martí, J., et al. 2013, *A&A*, arXiv:1309.3947

Table 2. The averaged orbital variability (20 bins) of LS I+61^o303.

phase bin	$EW(B)$	$EW(R)$	EW_B/EW_R	$EW(H\alpha)$	V	ΔV_p
	[\AA]	[\AA]	[\AA]	[\AA]	[mag]	[km s^{-1}]
0.00-0.05	4.780 \pm 0.306	6.392 \pm 0.343	0.7468 \pm 0.0229	11.173 \pm 0.629	10.7175 \pm 0.0189	336.07 \pm 4.28
0.05-0.10	5.138 \pm 0.193	6.256 \pm 0.135	0.8190 \pm 0.0212	11.409 \pm 0.295	10.7317 \pm 0.0129	327.17 \pm 2.43
0.10-0.15	4.558 \pm 0.304	5.775 \pm 0.256	0.7917 \pm 0.0377	10.380 \pm 0.460	10.7514 \pm 0.0172	338.61 \pm 3.22
0.15-0.20	5.241 \pm 0.140	6.096 \pm 0.151	0.8672 \pm 0.0271	11.337 \pm 0.237	10.7550 \pm 0.0121	341.30 \pm 3.24
0.20-0.25	5.415 \pm 0.201	6.074 \pm 0.162	0.8974 \pm 0.0351	11.489 \pm 0.311	10.7415 \pm 0.0142	344.92 \pm 4.01
0.25-0.30	5.342 \pm 0.270	5.990 \pm 0.161	0.8969 \pm 0.0450	11.332 \pm 0.343	10.7400 \pm 0.0146	339.69 \pm 4.96
0.30-0.35	5.503 \pm 0.219	6.036 \pm 0.252	0.9232 \pm 0.0349	11.539 \pm 0.428	10.7617 \pm 0.0083	328.42 \pm 4.34
0.35-0.40	7.245 \pm 0.497	6.517 \pm 0.398	1.1465 \pm 0.1090	13.402 \pm 0.690	10.7478 \pm 0.0066	312.95 \pm 7.86
0.40-0.45	6.163 \pm 0.313	6.326 \pm 0.227	0.9797 \pm 0.0408	12.354 \pm 0.480	10.7445 \pm 0.0112	321.89 \pm 5.93
0.45-0.50	6.247 \pm 0.473	7.274 \pm 0.513	0.8613 \pm 0.0304	13.521 \pm 0.962	10.7638 \pm 0.0105	319.35 \pm 11.4
0.50-0.55	6.274 \pm 0.356	8.173 \pm 0.274	0.7638 \pm 0.0297	14.084 \pm 0.580	10.7347 \pm 0.0078	324.87 \pm 10.0
0.55-0.60	5.565 \pm 0.206	7.194 \pm 0.237	0.7787 \pm 0.0234	12.490 \pm 0.371	10.7200 \pm 0.0187	336.06 \pm 7.74
0.60-0.65	5.231 \pm 0.201	7.147 \pm 0.173	0.7366 \pm 0.0236	12.238 \pm 0.337	10.7337 \pm 0.0165	336.23 \pm 4.30
0.65-0.70	5.212 \pm 0.218	7.935 \pm 0.384	0.6758 \pm 0.0293	13.148 \pm 0.545	10.7300 \pm 0.0113	353.55 \pm 4.16
0.70-0.75	4.563 \pm 0.273	6.637 \pm 0.363	0.6536 \pm 0.0507	11.270 \pm 0.517	10.7231 \pm 0.0122	345.93 \pm 4.87
0.75-0.80	4.829 \pm 0.310	6.892 \pm 0.226	0.6101 \pm 0.0685	11.433 \pm 0.507	10.7240 \pm 0.0119	339.71 \pm 5.57
0.80-0.85	4.416 \pm 0.265	6.274 \pm 0.251	0.6291 \pm 0.0622	10.435 \pm 0.452	10.7107 \pm 0.0158	344.06 \pm 5.48
0.85-0.90	4.485 \pm 0.226	6.740 \pm 0.289	0.6651 \pm 0.0184	11.197 \pm 0.464	10.7140 \pm 0.0111	333.27 \pm 4.36
0.90-0.95	4.480 \pm 0.232	6.478 \pm 0.273	0.6915 \pm 0.0203	10.626 \pm 0.516	10.7221 \pm 0.0123	343.30 \pm 6.78
0.95-1.00	4.628 \pm 0.274	6.212 \pm 0.245	0.7373 \pm 0.0221	10.601 \pm 0.534	10.7100 \pm 0.0116	338.96 \pm 4.48